



A MODELLING TOOL FOR DYNAMIC ANALYSIS OF MASONRY COLLAPSE MECHANISMS

A. Mehrotra ⁽¹⁾, M.J. DeJong ⁽²⁾

⁽¹⁾ Doctoral research student, University of Cambridge, Department of Engineering, aam62@cam.ac.uk

⁽²⁾ Senior Lecturer, University of Cambridge, Department of Engineering, mjd97@cam.ac.uk

Abstract

Typical out-of-plane collapse mechanisms for unreinforced masonry structures have been well documented. During assessment, these collapse mechanisms are usually evaluated from a static perspective, in order to determine the ground acceleration which would activate the mechanism. As the structure can resist larger ground motions due to dynamic resistance that increases with the scale of the structure, a multiple of the static acceleration is often used in assessment. Alternatively, the dynamics of these nonlinear collapse mechanisms are approximated by a single-degree-of-freedom linear-elastic oscillator. However, there are limitations to the accuracy of this approximation. As an alternative, the equations of motion for potential collapse mechanisms can be solved directly using rocking dynamics. Deriving these equations can be cumbersome and time-consuming, particularly for structures with complicated geometries and mechanisms which may involve multiple elements in the kinematic chain. In this paper, a new tool is presented which uses a digital drawing of a masonry structure in typical CAD software to directly generate the relevant equations of motion for user-defined, or automatically generated, collapse mechanisms. These equations of motion are then solved in Matlab to generate overturning envelopes which predict the response of the structure for a range of pulse-type excitations. The tool is applied to assess potential collapse mechanisms of a typical church in order to prioritise potential intervention measures.

Keywords: Masonry; nonlinear dynamics; computational tools

1. Introduction

Typical failure of unreinforced masonry structures generally takes place in the form of both in-plane and out-of-plane collapse mechanisms. Between the two, out-of-plane collapse is perhaps the most common mode of failure – especially in the case of masonry walls and façades such as those found in ordinary buildings. These out-of-plane collapse mechanisms have been well-documented ([1], [2]) and range from simple overturning of the façade and corner failure, to more complicated vertical arching mechanisms such as those observed in walls which are well-restrained at both the top and the bottom.

In the case of more complex unreinforced masonry structures, such as churches, local mechanisms involving macro-elements have again been found to dominate failure [3]. Several studies conducted over the last thirty years (e.g. [4]–[7]) have resulted in the compilations of the most frequently recurring collapse mechanisms found in Italian churches. One such catalog can be found in the official Italian church damage-survey form [8], portions of which can be found in Fig. 1. This catalog contains both simple mechanisms, such as overturning of the façade (1), gable (2), apse (16) and tip of the belfry spire (26), as well as more complicated mechanisms such as the collapse of the vault (5) and rocking of the belfry (28).

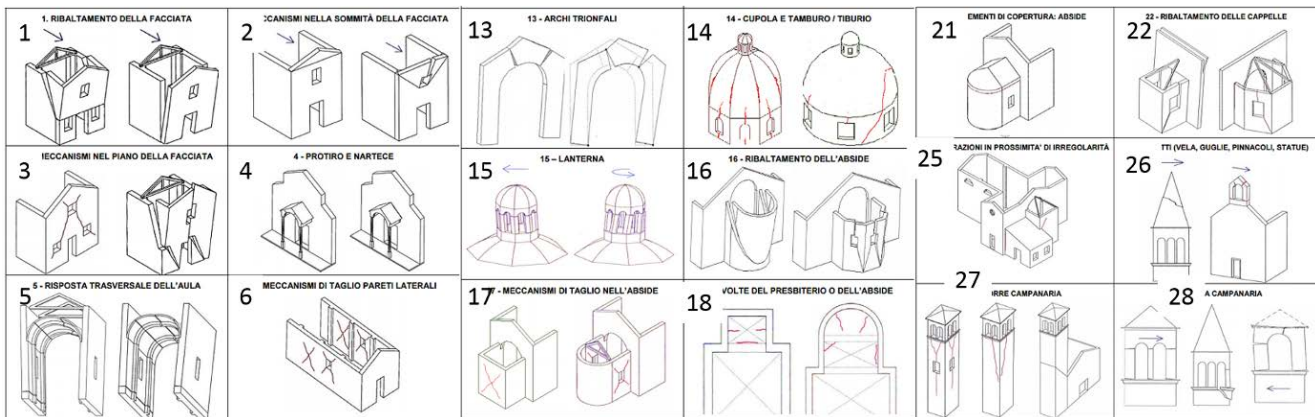


Fig. 1 – Typical church collapse mechanisms [8]

During assessment, these collapse mechanisms are generally analysed from a static perspective, with the objective of determining the ground acceleration which would cause the mechanism to occur [9]. The dynamic resistance of the structure, which increases with its scale, is factored into the assessment by using a multiple of the static acceleration. Alternatively, code-based procedures [9] allow a single degree of freedom linear elastic oscillator to be used to account for the dynamics of the nonlinear collapse mechanisms. These approximations incorporate some dynamic effects, but ignore others. As a result, they are un-conservative in some cases, but are over-conservative the majority of the time, often leading to expensive and potentially unnecessary retrofitting measures in churches and other historical masonry structures.

As an alternative, the equations of motion for potential collapse mechanisms can be derived directly using rocking dynamics, following the approach presented by Housner [10], who derived equations of motion for a single rigid rocking block, assuming that sliding and bouncing do not occur. Zhang and Makris [11] built on Housner's work by studying the rocking response to pulse-type excitations, which are known to be particularly destructive to rocking structures. Subsequently, closed-form solutions were derived for Housner's equation of motion for the rocking block when subjected to cycloidal pulses [12]. Analytical equations for non-dimensional overturning plots were also provided, so that the response of the block to any pulse-type ground motion could be readily-determined – needing only to be scaled by the intensity and frequency of the excitation [12].

Equations of motion have also been derived for structures with more complicated geometries such as masonry spires, portal frames, arches/vaults and asymmetric frames [13]–[16]. Structures such as the spire and portal frame, which have relatively simple mechanisms, have been found to exhibit direct dynamic equivalence to the single rocking block [16]. For more complicated mechanisms involving multiple elements in the kinematic



chain, such as masonry arches/vaults and asymmetric frames, the dynamic response was approximated using linearization of the equations of motion about the point of unstable equilibrium [16]. In the case of façades, equations of motion have also been derived to account for external loads in the form of additional masses such as floors/roof/beams, and external static forces in the form of vault and roof thrusts and tie bar reactions [17].

However, deriving these equations can be cumbersome and time-consuming, particularly for structures with complex geometries and mechanisms which involve multiple elements in the kinematic chain. In this paper, a new tool is presented which uses a digital drawing of a masonry structure in a typical CAD software to directly generate the relevant equations of motion for user-defined, or automatically generated, collapse mechanisms. These equations of motion are then solved in Matlab to generate overturning envelopes which predict the response of the structure to a range of pulse-type excitations (Fig. 2). The tool is applied to assess potential collapse mechanisms of a typical church geometry, based on San Leonardo Limosino church in Mortizzuolo, Italy, in order to prioritise potential intervention measures. A flowchart illustrating the functioning of this tool can be found in Fig. 3. Only pulse-type excitations are considered in this study to demonstrate the tool and compare mechanisms, but full time history response could also be conducted using the same framework.

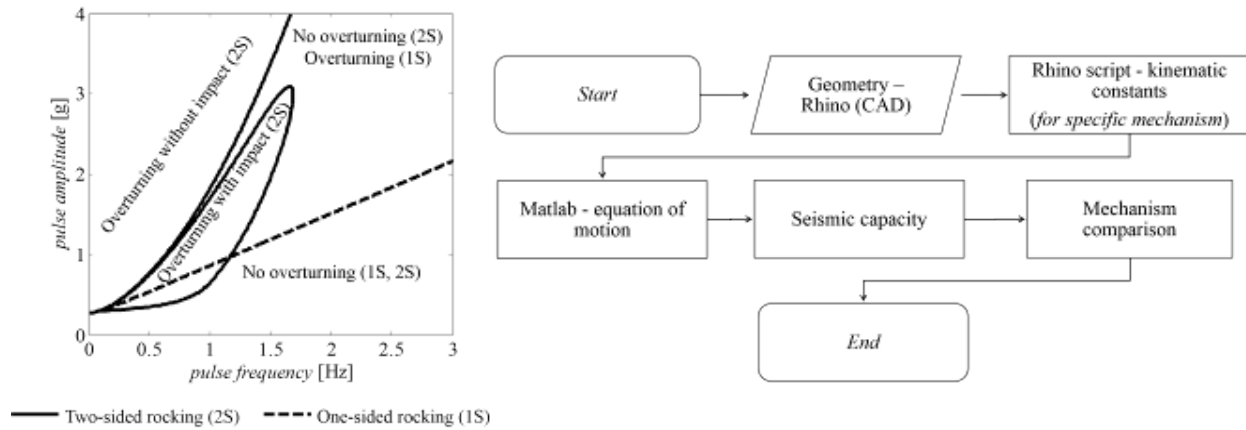


Fig. 2 – Sample overturning envelope for both one and two-sided rocking

Fig. 3 – Flowchart demonstrating modelling procedure

2. Methodology

2.1 Derivation of equation of motion using Rhino script

All the equations of motion for the different structural geometries and mechanisms assume the following general linearized form, with linearization occurring about the point of unstable equilibrium ($\phi = \phi_{cr}$) in order to obtain local dynamic equivalence with the rocking block:

$$\tilde{I}\ddot{\phi} - \tilde{K}(\phi - \phi_{cr}) = -\tilde{B}\ddot{u}_g + \tilde{M} \quad (1)$$

Where \tilde{I} is the moment of inertia of the structure about the axis of rotation, \tilde{M} is the generalized force provided by the external static forces, ϕ_{cr} is the critical rotation, and \tilde{K} and \tilde{B} are constants specific to the kinematics of the unstable equilibrium configuration. Using the following transformation of variables:

$$\theta = \phi \frac{\tilde{K}}{g\tilde{B}} \quad (2)$$

Eq. (1) can be rewritten as:

$$\ddot{\theta} = p_{eq} \left(\theta - \tilde{\lambda} - \frac{\ddot{u}_g}{g} \right) \quad (3)$$



Where p_{eq} is the equivalent frequency parameter:

$$p_{eq} = \sqrt{\frac{\tilde{K}}{\tilde{I}}} \quad (4)$$

And $\tilde{\lambda}$ is an approximation of the static load multiplier which activates the mechanism:

$$\tilde{\lambda} = -\frac{\tilde{M} - \tilde{K}\phi_{cr}}{g\tilde{B}} \quad (5)$$

Furthermore, the coefficient of restitution η , which measures the energy dissipated during impact, also needs to be calculated. This was assumed to be a function of the geometry of the structure and is calculated using conservation of moment of momentum about the axis of rotation. For the case of two-sided rocking, a generalized form of the equation proposed by Housner [10] is used, as shown in Eq. (6), while for the case of one-sided rocking (most commonly observed in façades), a generalized version of the equation proposed by Sorrentino et al. [18] is used, as shown in Eq. (7) - in both cases for mechanisms which can fundamentally be considered as a single rocking block.

$$\eta_{2s} = 1 - 2\frac{p^2 R}{g} \sin^2 \alpha \quad (6)$$

$$\eta_{1s} = \left(1 - 2\frac{p^2 R}{g} \sin^2 \alpha\right)^2 \left(1 - 2\frac{p^2 R}{g} \cos^2 \alpha\right) \quad (7)$$

In Equations (6) and (7), p is the frequency parameter, R is the radius of rotation and α is the slenderness of the block. The analytical formulae for the coefficients of restitution for more complex mechanisms have also been considered, but have not been provided here in the interest of brevity.

Thus the terms p_{eq} , $\tilde{\lambda}$ and η are the resultant kinematic constants defining the equation of motion of the mechanism, and can be derived solely based on the geometry of the structure. To this end, scripts have been written in Rhino which can compute these kinematic constants for a range of different mechanisms, for user-defined structural geometries of varying complexity. As input, upon opening the CAD file and calling the appropriate script, the user need only select the objects involved in the mechanism, draw the axis of rotation and any cracks which occur, and in the case of the façade mechanism, select or input any additional masses or forces. When necessary, the user will also be prompted to specify whether the mechanism under consideration is one-sided or two-sided. The script will then automatically calculate the resultant kinematic constants, which are exported to Matlab where they are used to generate and solve the corresponding equation of motion.

2.2 Solution to equations of motion and overturning envelope generation

The equations of motion exported to Matlab are solved using the closed-form solutions derived by Dimitrakopoulos and DeJong [12] for pulse-type excitations. These results are then used to generate overturning plots (Fig. 2), which predict whether or not the structure will overturn via the given mechanism for a range of pulse frequencies and amplitudes, and also indicate if overturning occurs with or without impact.

Nonetheless, solving these equations can be time-consuming, especially if the objective is to create multiple overturning envelopes in order to rapidly compare the relative dynamic resilience of different collapse mechanisms. Given that the derived equations have local dynamic equivalence with a simple rocking block, a library of dimensionless overturning plots was instead pre-generated for a single block, for a range of coefficients of restitution, for both one and two-sided rocking. Based on the mechanism under consideration (one-sided vs two-sided rocking) and the value of the coefficient of restitution η exported to Matlab, the corresponding dimensionless overturning plot is extracted from the library and simply scaled by p_{eq} and λ , thus saving a considerable amount of time and computational effort.

Furthermore, given that a number of mechanisms take place at a height above the ground level, dynamic amplification of the ground motion also needs to be accounted for. In order to do this, elastic modal analysis is employed whereby response spectra are generated by solving the equation of motion for a single-degree-of-freedom system with 5% damping and a natural frequency f_n corresponding to that of the structure under consideration, when subjected to single sine pulses with a range of different frequencies (f_p). As the objective is to use a relatively simple amplification model, only first-mode response is considered, without taking into account higher mode effects. The resultant response spectrum is obtained by plotting the variation of the maximum recorded acceleration a_r (normalized by the input/ground acceleration a_g), with the normalized pulse frequency (f_p/f_n), as illustrated by Fig. 4a. The response acceleration a_r generally acts at the modal height h_e , but mechanisms could occur either above or below this point. Thus, assuming a linear variation of the response acceleration with height such as that used by Priestley [19] (Fig. 4b), the resulting scaled acceleration a_{sc} at a given height h can be computed, and the linear-elastic pulse response spectrum for the building can then be modified accordingly for a given height within the structure (Fig. 4c). This modified linear-elastic pulse response spectrum can then be used to scale the corresponding overturning plots in Matlab. Note that only the pulse response is considered in this paper, but a similar procedure could be used when considering the response to a full earthquake time-history.

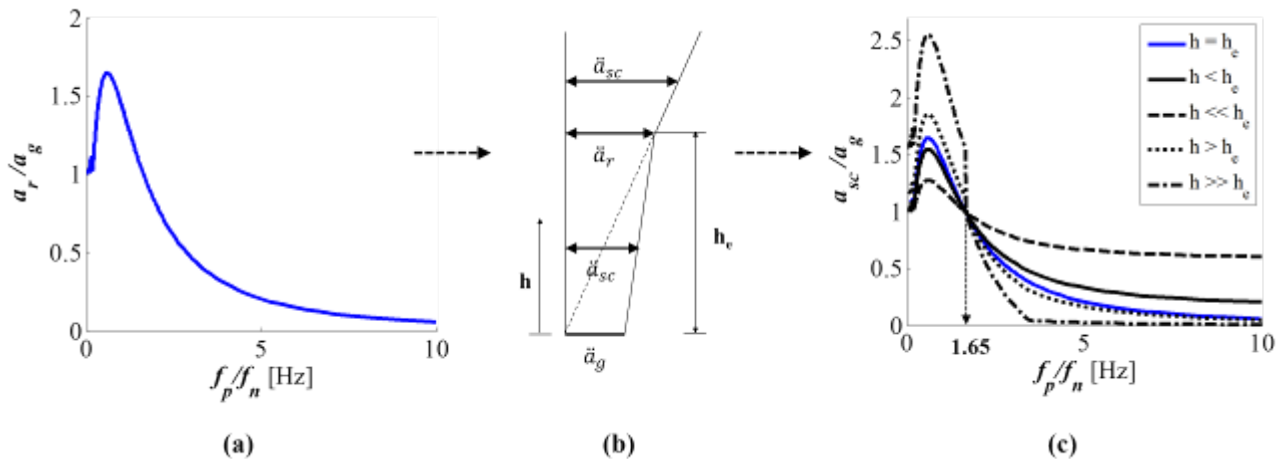


Fig. 4 – Generation of scaled pulse response spectra (PRS): (a) original PRS; (b) variation of response acceleration with height; (c) scaled PRS.

3. Case Study: Church of San Leonardo Limosino

To illustrate the potential use of this tool, the Italian church of San Leonardo Limosino was chosen as a case-study. The church was constructed in the 15th century and comprises a nave and side aisles (which are covered by cross-vaults), a roof supported by king-post trusses, a rounded apse, and a bell tower [20]. During the 2012 Emilia earthquakes, the church suffered a significant amount of damage - during the first shock on May 20th, the tip of the bell tower's spire collapsed and a portion of the façade above the central window overturned out-of-plane (Fig. 5a). Vertical cracks below the spire and some corner spalling just above the roof level of the church were also observed in the bell tower [20]. During the second shock on May 29th, the façade suffered further damage, while the portion of the bell tower above the roof level of the church completely collapsed (Fig. 5b).

In order to analyze the church using the tool, a 3D CAD drawing of the structure was first created in Rhino based on the dimensions and drawings presented in Decanini et al. [20]. The scripts in Rhino were then run for both the actual mechanisms observed (Fig. 6a) and the potential mechanisms which could have occurred (Fig. 6b), the selection of which was based on the presence of certain macroelements within the church. Parametric studies were also conducted for some of these mechanisms. Factors such as the location of the axis of rotation and crack angle were varied, and in the case of the façade additional loading from the vaults and roof were considered. The kinematic constants computed for each of these mechanisms were then exported to Matlab and were used to generate the corresponding (unscaled) overturning envelopes.



Fig. 5 – Church of San Leonardo Limosino after the (a) 20th May 2012 shock; (b) 29th May 2012 shock [3]

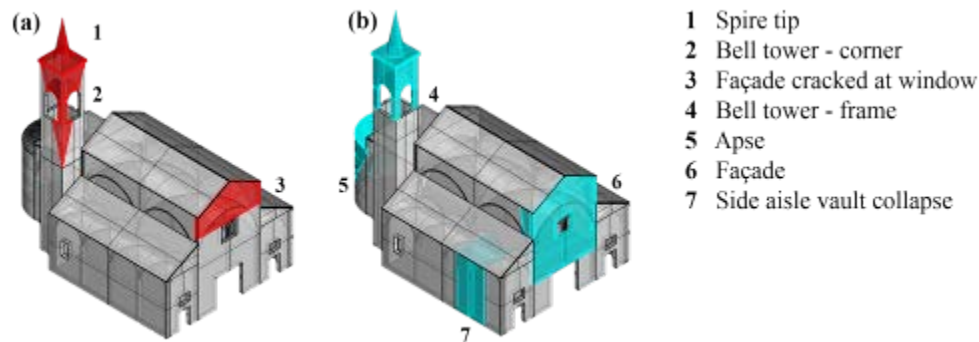


Fig. 6 – Collapse mechanisms considered: (a) actual mechanisms; (b) potential mechanisms

To generate the pulse response spectra necessary for the scaling of these overturning envelopes (to account for dynamic amplification effects), the natural frequency of the structure also needed to be determined. The bell tower was assumed to be free-standing (i.e. independent of the church) and its natural frequency was approximated as 5.2 Hz using Lord Rayleigh’s principle as in [13]. For the main church body, a natural frequency of 2.9 Hz was estimated based on several finite element analyses conducted on churches of similar scale ([21]–[26]). The modal heights were also calculated, and were found to be 14.46 m and 6.64 m for the bell tower and church respectively. Using the computed natural frequencies and modal heights, the pulse response spectra and consequently the scaled overturning envelopes were generated, with the latter being presented in the following section.

4. Results

In the case of the masonry spire of the bell tower (Mechanism 1, Fig. 6a), two-sided rocking was assumed, and overturning plots were generated for both varying crack angles (Fig. 7a, with the angle being measured from the horizontal) and varying crack heights (Fig. 7b, with the height being measured from the tip of the spire). From Fig. 7a it can be seen that increasing the angle of the crack tends to decrease the stability of the spire, thus making it more vulnerable to overturning for all pulse frequencies, while Fig. 7b illustrates that increasing the height of the portion that separates and rocks tends to increase the stability of the spire, thus making it less vulnerable to overturning. In reality, the crack angle would be limited by the coursing of the masonry.

In the case of the apse (Mechanism 5, Fig. 6b), one-sided rocking was assumed and overturning envelopes were generated for varying crack angles (measured from the horizontal), with the cracks occurring at both the base of the apse as well as the window openings (Fig. 8). As Fig. 8 illustrates, the mechanisms originating at the window openings are, for the most part, more susceptible to overturning, and in general the overturning vulnerability increases with an increase in crack angle. However, in the case of the crack angle of 45°, the mechanism originating at the base is more likely to overturn for the higher frequencies (> 3 Hz) as well as for frequencies less than 1 Hz. Similar trends can also be observed for the larger crack angles – whereby the difference between the base and window plots tends to decrease with an increase in pulse frequency, with the two plots eventually “crossing-over” and switching relative vulnerabilities at higher frequencies.

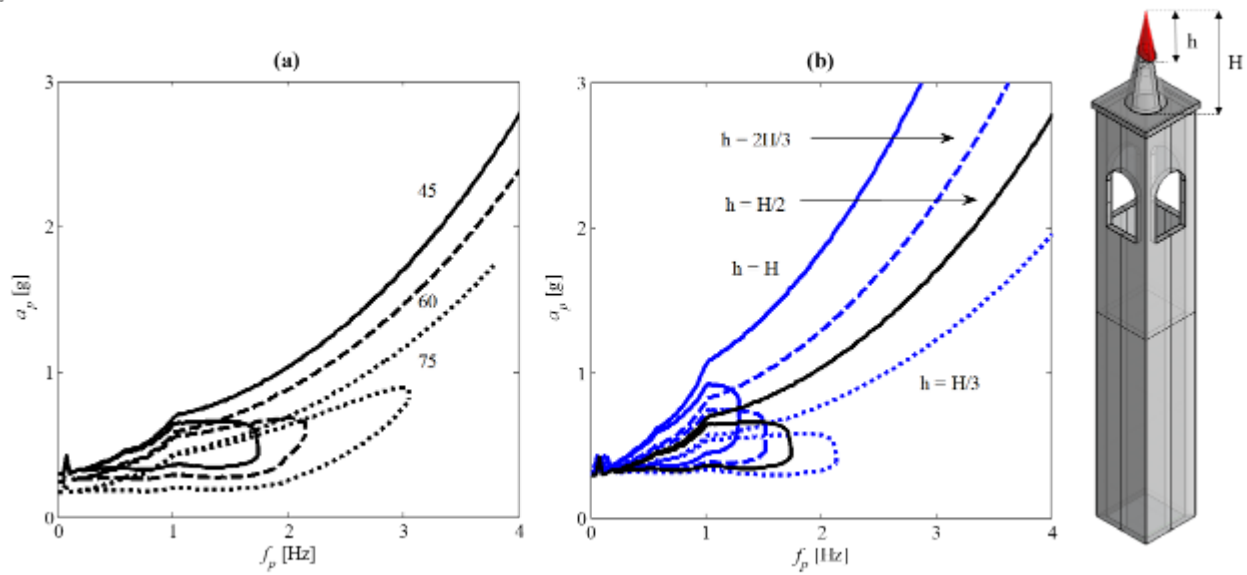


Fig. 7 – Spire overturning envelopes: (a) varying crack angles at $h = H/2$; (b) varying heights for a constant crack angle of 45°

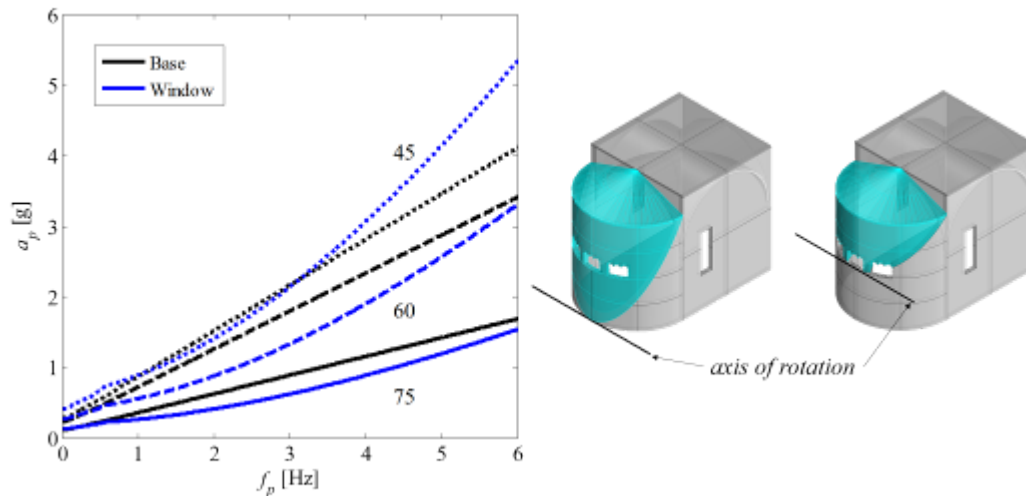


Fig. 8 – Apse overturning envelopes for varying crack angles, with crack starting from base (black) and window openings (blue)

In the case of the façade, five different mechanisms were evaluated, as illustrated by Fig. 9. One-sided rocking was assumed for all cases, and from the resulting overturning plots it was found that for all considered frequencies, Case 1 (gable only) was the least vulnerable to overturning, while Case 4 (façade + side walls + additional loads) was the most vulnerable. Cases 2, 3 and 5 demonstrated relatively similar dynamic resilience in the frequency range of 1 – 5 Hz.

In the case of the bell tower, corner mechanisms were evaluated at both the mid-height of the tower as well as at the belfry window (Mechanism 2, Fig. 6a). The belfry was also evaluated as a portal frame (Mechanism 4, Fig. 6b) with the mechanism taking the form illustrated in Fig. 10. Two-sided rocking was assumed for all three mechanisms, while in the case of the corner mechanisms one-sided rocking was also investigated. The overturning plots for these mechanisms can be found in Fig. 10. From Fig. 10 it can be seen that for pulse frequencies between 0.5 - 2.5 Hz the portal frame mechanism appears to control collapse, while for frequencies greater than 2.5 Hz and less than 0.5 Hz the corner mechanism originating at the midpoint tends to dominate. Furthermore, for all frequencies, the corner mechanism (both one and two-sided) originating at the belfry window demonstrates greater dynamic resilience than its mid-height counterpart.

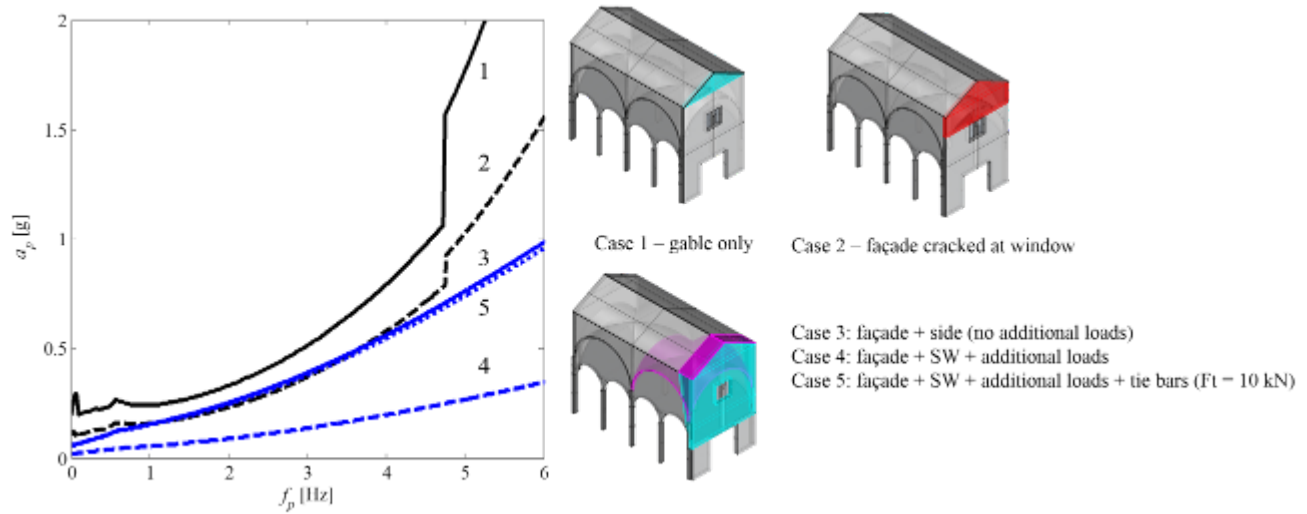


Fig. 9 – Façade overturning envelopes for different cases

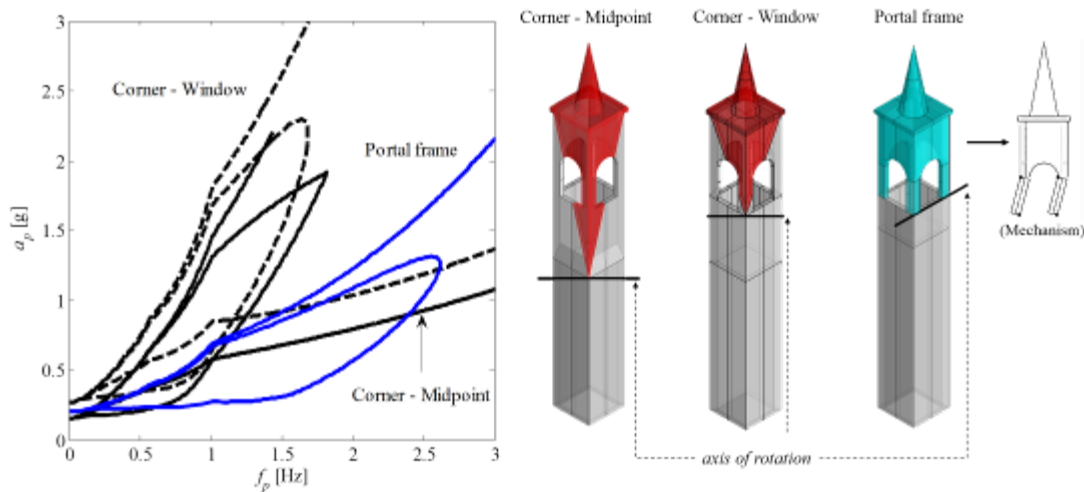


Fig. 10 – Bell tower overturning envelopes for different mechanisms. One-sided and two-sided envelopes are shown for the corner collapse mechanisms, while only the two-sided mechanism is shown for the portal frame.

Assuming one-sided rocking, overturning envelopes were also generated for the three-block mechanisms involving the vault of the side-aisle (Mechanism 7, Fig. 6b) as illustrated by Fig. 11, with the mechanisms being evaluated at both the base of the side wall and the mid-height. The overturning envelopes in this case assume a relatively linear form - the resistance to overturning generally increases with an increase in pulse frequency, with the mechanism originating at the base displaying a larger vulnerability to overturning for all frequencies.

In order to compare the relative dynamic resilience of the different collapse mechanisms, the controlling mechanisms from each of the considered cases were plotted in Fig. 12, with the only exception being the façade, where Case 2 was plotted instead of Case 4, as that was the mechanism which was actually observed. Furthermore, in order to highlight the effect of ground motion (dynamic) amplification, both the unscaled (Fig. 12a) and scaled (Fig. 12b) overturning envelopes were plotted. From Fig. 12 it can be seen that for both the scaled and unscaled cases the façade mechanism appears to be the most vulnerable to overturning, followed by the spire mechanism for frequencies less than 2 Hz (unscaled) and 2.5–3 Hz (scaled), while the side-aisle exhibits the greatest resistance to overturning for all frequencies. Fig. 12 also reveals that accounting for dynamic amplification generally reduces the minimum pulse amplitude required for overturning and in some cases even changes the relative vulnerabilities of the different collapse mechanisms.

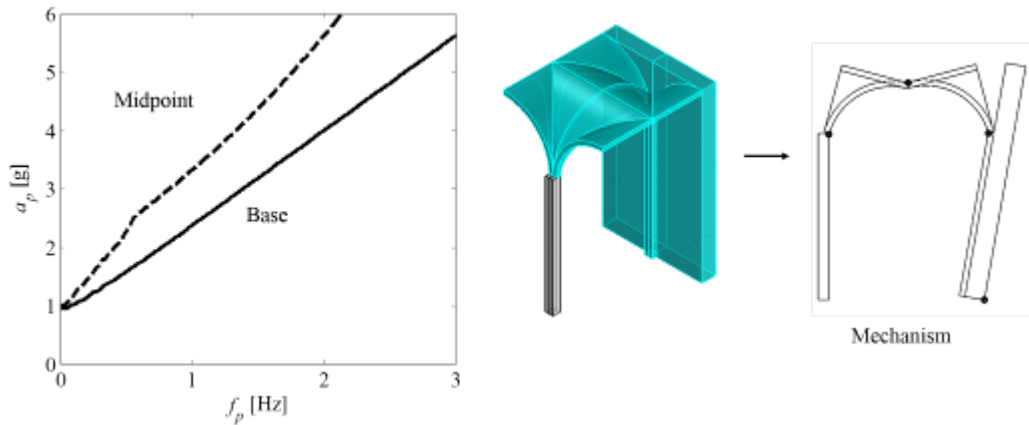


Fig. 11 – Side aisle overturning envelopes and (three-block) mechanism

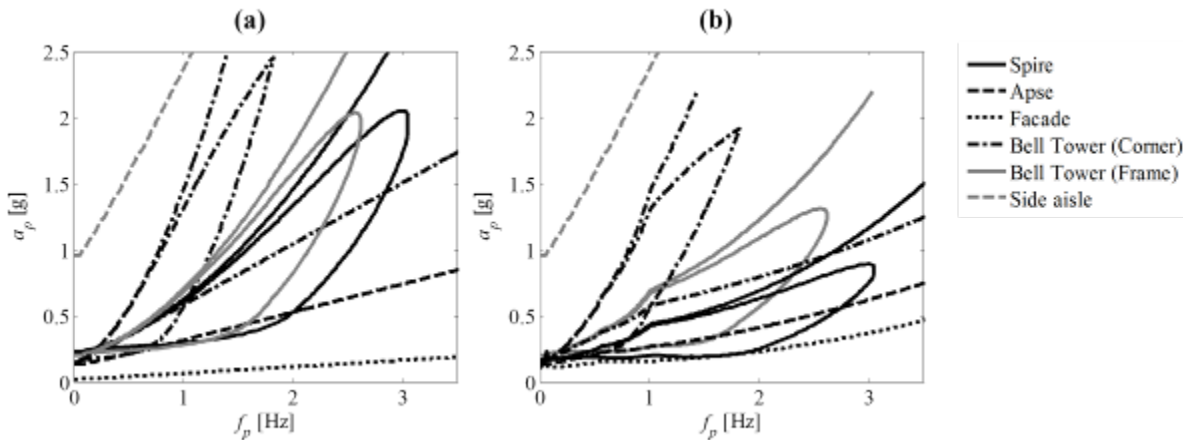


Fig. 12 – Comparison of overturning plots for different mechanisms: (a) without and (b) with amplification

5. Discussion

5.1 Effect of slenderness and scale

The resistance of objects to overturning is dependent on both their slenderness and scale. While the ratio of the acceleration amplitude of the ground motion to the slenderness of a structure determines when rocking initiates, the magnitude of rotation (and thus collapse) depends on the scale of the structure with respect to the period of large pulses within the ground motion. Typically, larger structures require a longer pulse in order to generate enough rotational momentum to overturn, while smaller objects could potentially overturn for shorter pulses as well.

The effect of slenderness and scale on the rocking stability of structures is illustrated by the overturning envelopes generated for the spire (Fig. 7). From Fig. 7a it can be seen that for a constant crack height, the resistance of the spire to overturning decreases with an increase in crack angle. An increase in crack angle results in an increased slenderness of the structure, thus leading to rocking initiating earlier. Furthermore, these more slender structures are also of a relatively smaller scale than their stockier counterparts and are thus susceptible to multiple-impact overturning for higher frequencies as well. This effect of scale on stability is reinforced by Fig. 7b, wherein for a constant crack angle and varying crack heights – that is, for a constant slenderness and varying scale - it can be seen that the overturning resistance again decreases with a decrease in scale.

For two-sided rocking mechanisms involving structures of similar scale but different slenderness, such as the two corner mechanisms (Fig. 10), it can be seen that for more slender structures (in this case the mechanism which initiates at the tower midpoint) rocking not only initiates earlier, but overturning for both the multiple and



no impact cases occurs at a lower pulse amplitude. However, as the mechanisms involve structures of relatively similar scale, the range of pulse frequencies for which multiple impact overturning occurs remains unchanged.

For one-sided rocking mechanisms, such as those observed in the apse and façade walls (Fig. 8 and Fig. 9 respectively) only positive pulse overturning without impact is considered. In this case, the only variation observed is the pulse amplitude at which overturning occurs. For the façade and its associated mechanisms, resistance to overturning was generally found to decrease with an increase in slenderness, with the gable (Case 1) being the stockiest and hence the least susceptible to overturning. However, Case 2, despite being less slender than Case 3, was found to display similar dynamic resilience to the latter, and in some cases was even observed to be more susceptible to overturning. This behavior is due to amplification of the ground motion, which shall be discussed in greater detail in the following sub-section.

For the apse, the threshold pulse amplitudes at which overturning occurs were again found to decrease with an increase in slenderness. However, in the case of the 45° crack angle, the mechanism originating at the window, despite its smaller scale, was largely found to be more resistant to overturning than the corresponding base mechanism. This is due to the fact that the slenderness of the structure only controls the minimum acceleration (for an infinitely long pulse) required for overturning to occur, while the rate at which this increases for higher frequency pulses depends on the ratio between λ , which is linked to the slenderness, and p_{eq} , which is related to the scale. For the crack angle of 45°, the window mechanism was not only stockier than the base (0.41 vs 0.29 rad), but also had a higher ratio of λ to p_{eq} (0.24 vs 0.21), thus resulting in a generally higher resistance to overturning. However, the window mechanism also occurs at a height above the ground, and, like the façade, experiences amplification of the ground motion which reduces the overturning resistance, making it more vulnerable than the base mechanism for lower frequencies – especially in the range of 1 – 3 Hz.

5.2 Elastic amplification and de-amplification

As a number of the mechanisms considered in this study occur above the ground level, amplification effects needed to be accounted for as they tend to increase the overturning vulnerability of the structure. As discussed in section 2.2, this was done using pulse response spectra (Fig. 4) which were generated and scaled according to the height at which the mechanisms occurred. From Fig. 4c it can be seen that amplification of the ground motion occurs for $f_p < 1.65 f_n$, while de-amplification occurs for $f_p > 1.65 f_n$, with both amplification and de-amplification effects being more pronounced at heights greater than the modal height of the structure (Fig. 4c). Note that the simplified procedure utilized here is meant to demonstrate amplification and de-amplification effects depending on the natural frequency of the structure, but needs refinement before practical use.

The effects of elastic amplification on one-sided mechanisms are best illustrated by the façade ($f_n = 2.9$ Hz) overturning envelopes (Fig. 9), where the gable mechanism (Case 1), which occurs well above the modal height, undergoes the greatest amplification/de-amplification compared to Cases 2 and 3, which occur at lower heights. The “jumps” in the graphs representing the increase in stability due to de-amplification occur at $f_p = 1.65 f_n = 4.8$ Hz. Elastic de-amplification can also be used to explain the “switch” in relative vulnerabilities of the apse overturning envelopes at higher frequencies. Note that this jump is solely a result of the approximate method used for amplification and de-amplification, but needs further consideration. Elastic amplification also accounts for the fairly comparable overturning vulnerabilities of Cases 2 and 3 of the façade. As Case 2 occurs at a greater height than Case 3, it has greater amplification of the ground motion for frequencies less than $1.65 f_n$ and consequently a greater increase in vulnerability to overturning. Correspondingly, the reduction of the overturning resistance of the 45° apse window mechanism can also be attributed to the effect of elastic amplification for frequencies less than 4.8 Hz. In the case of two-sided mechanisms, the effects of elastic amplification are illustrated by Fig. 12. If amplification effects are not considered (Fig. 12a), both the spire and the belfry (frame) have relatively similar vulnerabilities. However, accounting for elastic amplification (Fig. 12b) results in a greater increase in vulnerability of the spire than of the belfry, as this mechanism occurs at a greater height than the frame mechanism, and as such experiences a greater amplification of the ground motion.

5.3 Effect of reinforcement

The overturning envelopes generated in Fig. 9 also highlight the effect of reinforcement on the dynamic resilience of the façade. From Fig. 9 it can be seen that the addition of the tie bars to Case 4 effectively countered



the influence of the additional loads from the roof and thrust from the vault, resulting in the structure having an overturning vulnerability comparable to the case in which there were no additional loads at all. In fact, it could very well be the case that such reinforcement, which ensures good connectivity between the façade and side walls, does actually exist (either directly or through quality masonry with interlocking at the wall intersection) and prevented Case 4 from taking place in reality, thus making Case 2 the most vulnerable mechanism for the façade (as observed in the damage).

5.4 Comparison with field observations

Comparing the results from Fig. 12 to the findings of the post-earthquake damage surveys ([3], [20]) it can be seen that there is a generally good correlation between the predictions of the overturning plots and results of the field inspections. Fig. 12 predicts that for frequencies less than 3 Hz, the most likely or vulnerable mechanisms are the out-of-plane collapse of the portion of the façade above the window, and the overturning of the bell tower spire. In reality, both these mechanisms took place during the first shock of the Emilia earthquake in 2012. After this first shock, some corner spalling of the bell tower had also been observed [20], which could potentially have weakened the structure, thus making it more susceptible to corner failure during the second shock.

6. Conclusions

In this paper a new tool to assess and compare the relative vulnerabilities of different masonry collapse mechanisms is presented. Using a CAD drawing of a typical church geometry, which was based on the Italian Church of San Leonardo Limosino, the tool was used to derive equations of motion for various mechanisms, and solve for their response to pulse-type excitations, while taking into account elastic amplification of the ground motion. The resulting overturning envelopes predict the response of each mechanism to a range of pulse frequencies and amplitudes. Generally, good agreement was observed between the analysis results and field observations, with the overturning plots predicting the highest vulnerability for the portion of the façade above the window and the spire of the bell tower, which both collapsed in the earthquake. For the façade in particular, the plots illustrate the beneficial effect of connectivity of elements on the seismic resilience of the structure.

The effect of slenderness and scale on the rocking stability of the church was also evaluated. For both one and two-sided mechanisms, the slenderness was observed to control the point at which rocking initiates as well as the minimum acceleration required for very long-period pulses to cause overturning. For two-sided mechanisms, the scale of the macro-element involved in the rocking mechanism was found to govern the range of pulse frequencies for which multiple-impact overturning could occur, while for one-sided mechanisms the ratio of slenderness to scale determined the rate at which the structure's resistance to overturning increased with an increase in pulse frequency. The overturning plots also demonstrated that elastic amplification and de-amplification can have a significant effect when evaluating which mechanism is most critical. However, the simplified procedure used in this paper to account for amplification/de-amplification requires further refinement.

7. Acknowledgements

Financial support for this research was provided by the Jawaharlal Nehru Memorial Trust in conjunction with the Cambridge Commonwealth, European & International Trust.

8. References

- [1] D'Ayala D, Speranza E (2002): An Integrated Procedure for the Assessment of Seismic Vulnerability of Historic Buildings. *Proceedings of the 12th European Conference on Earthquake Engineering*, London, UK.
- [2] D'Ayala D, Speranza E (2003): Definition of Collapse Mechanisms and Seismic Vulnerability of Historic Masonry Buildings. *Earthquake Spectra*, **19**(3), 479–509.
- [3] Sorrentino L, Liberatore L, Decanini LD, Liberatore D (2014): The performance of churches in the 2012 Emilia earthquakes. *Bulletin of Earthquake Engineering*, **12**(5), 2299–2331.
- [4] Giuffrè A (1988): Restauro e sicurezza in zona sismica. La Cattedrale di S. Angelo dei Lombardi. *Palladio*, **1**, 95–120.



- [5] Doglioni F, Moretti A, Petrini V, Eds. (1994): *Le chiese e il terremoto: dalla vulnerabilità constatata nel terremoto del Friuli al miglioramento antisismico nel restauro, verso una politica di prevenzione*. Lint Editoriale.
- [6] Lagomarsino S (1998): A new methodology for the post-earthquake investigation of ancient churches. *11th European Conference on Earthquake Engineering*, Paris, France.
- [7] Lagomarsino S, Podestà S, Cifani G, Lemme A (2004): The 31st October 2002 earthquake in Molise (Italy): a new methodology for the damage and seismic vulnerability survey of churches. *13th World Conference on Earthquake Engineering*, Vancouver, Canada.
- [8] PCM-DPC MiBAC (Presidenza Consiglio dei Ministri - Dipartimento della Protezione Civile Ministero Beni e Attività Culturali) (2006): Model A-DC Scheda per il rilievo del danno ai beni culturali - Chiese.
- [9] NTC (2008): Decreto Ministeriale 14/1/2008. Norme tecniche per le costruzioni. Ministry of Infrastructures and Transportations. G.U.S.O n.30 on 4/2/2008.
- [10] Housner GW (1963): The Behavior of Inverted Pendulum Structures during Earthquakes. *Bulletin of the Seismological Society of America*, **53**(2), 403–417.
- [11] Zhang P, Makris N (2001): Rocking response of free-standing blocks under cycloidal pulses. *Journal of Engineering Mechanics*, **127**, 473–483.
- [12] Dimitrakopoulos EG, DeJong MJ (2012): Revisiting the rocking block: closed-form solutions and similarity laws. *Proc. R. Soc. A Math. Phys. Eng. Sci.*, **468**(2144), 2294–2318.
- [13] DeJong MJ (2012): Seismic response of stone masonry spires: Analytical modeling. *Engineering Structures*, **40**, 556–565.
- [14] Makris N, Vassiliou MF (2013): Planar rocking response and stability analysis of an array of free-standing columns capped with a freely supported rigid beam. *Earthquake Engineering & Structural Dynamics*, **42**(3), 431–449.
- [15] De Lorenzis L, DeJong MJ, Ochsendorf JA (2007): Failure of masonry arches under impulse base motion. *Earthquake Engineering & Structural Dynamics*, **36**(14), 2119–2136.
- [16] DeJong MJ, Dimitrakopoulos EG (2014): Dynamically equivalent rocking structures. *Earthquake Engineering & Structural Dynamics*, **43**(10), 1543–1563.
- [17] Mauro A, de Felice G, DeJong MJ (2015): The relative dynamic resilience of masonry collapse mechanisms. *Engineering Structures*, **85**, 182–194.
- [18] Sorrentino L, Al Shawa O, Decanini LD (2011): The relevance of energy damping in unreinforced masonry rocking mechanisms. Experimental and analytic investigations. *Bulletin of Earthquake Engineering*, **9**(5), 1617–1642.
- [19] Priestley MJ (1985): Seismic behaviour of unreinforced masonry walls. *Bulletin of the New Zealand Society of Earthquake Engineering*, **18**(2), 191–205.
- [20] Decanini LD, Liberatore D, Liberatore L, Sorrentino L (2012): Preliminary Report on the 2012, May 20, Emilia Earthquake, v.1.
- [21] Casarin F, Modena C (2008): Seismic Assessment of Complex Historical Buildings: Application to Reggion Emilia Cathedral, Italy. *International Journal of Architectural Heritage*, **2**(3), 304–327.
- [22] Betti M, Vignoli A (2008): Modelling and analysis of a Romanesque church under earthquake loading: Assessment of seismic resistance. *Engineering Structures*, **30**(2), 352–367.
- [23] Betti M, Vignoli A (2011): Numerical assessment of the static and seismic behaviour of the basilica of Santa Maria all’Impruneta (Italy). *Construction and Building Materials*, **25**(12), 4308–4324.
- [24] Mele E, De Luca A, Giordano A (2003): Modelling and analysis of a basilica under earthquake loading. *Journal of Cultural Heritage*, **4**, 355–367.
- [25] Castellazzi G, Gentilini C, Nobile L (2013): Seismic Vulnerability Assessment of a Historical Church : Limit Analysis and Nonlinear Finite Element Analysis. *Advances in Civil Engineering*. **2013**, 1-12.
- [26] Dal Cin A, Russo S (2014): Influence of the annex on seismic behavior of historic churches. *Engineering Failure Analysis*, **45**, 300-313.